Glider Fuselage-Wing Junction Optimization using CFD and RBF Mesh Morphing

Introduction

The state-of-the-art engineering design are today mainly based on multiobjective multiphisics optimization procedures in which several numerical methods interact in a common environment. The task is to automatically drive the selection of the "optimum" combination of the parameters that define the design space of the problem under investigation. The efficiency of such procedures, which might become very complex, is strongly related to the efficiency of the single numerical tool and to the designer capability to properly setup the design problem.

Some of the most critical aspects in automatic optimization procedures, particularly felt in aerodynamic design problems, are the parameterization of the geometries and the update on the computational domain. A very efficient way to face both aspects is to directly act on the Computation Fluid Dynamics (CFD) grid applying mesh morphing techniques.

This paper describes a mesh morphing based on RBF numerical optimization procedure, developed to be used for aerodynamic design, and its application on a typical aeronautical design problem.

Shape optimization through RBF mesh morphing technique

RBF are a class of mathematical interpolation functions that, in Computer-Aided Engineering (CAE) applications, can be used to drive mesh morphing (smoothing) of the discretized domain of the computational model applying predefined displacements to a set of purposely generated points, called source points (Figure 1).

Figure 1 Set up step of the RBF Morph example. The morphed action is limited in the box region "domain 1" (left). The motion of the surfaces inside the encapsulation domain (right) is imposed to the points on the windshield (fixed), the fairing (fixed) and the helmet (moving).

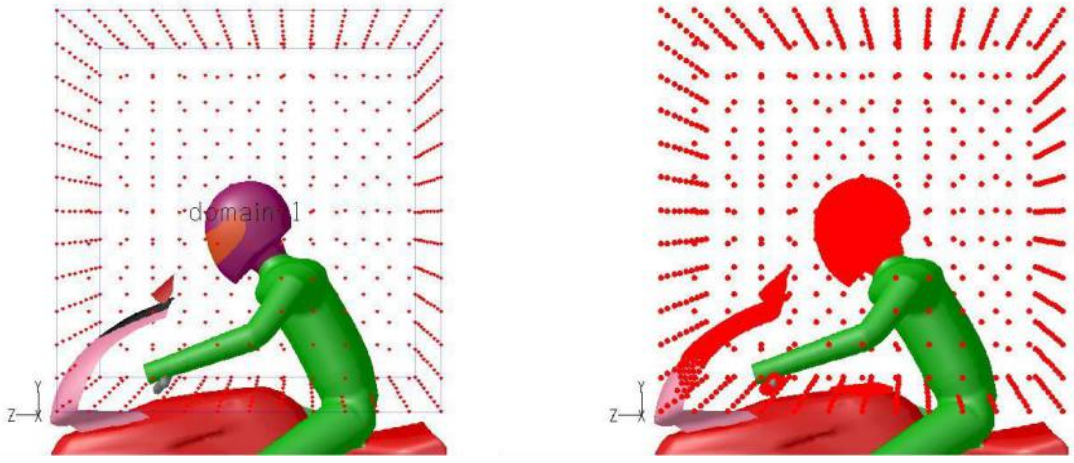

The main characteristics of such an approach are the meshless property, the preservation of mesh consistency and the low disk usage in addition to standard calculation, whilst some among its main advantages are the exact control of nodes during smoothing, the prevention of remeshing noise, the possibility to be fully integrated in the computing process and the high performance in handling large models. Despite all the aforementioned benefits there are still some open issues that are limiting the excellent potential of mesh morphing in general and in RBF mesh morphing in the specific. The first limit is given by mesh distortion occurring after morphing. Even if it can be alleviated using smooth morpher (and RBF based on bi-harmonic kernel are a good example) there are applications that cannot be faced reusing the same mesh for topological or room reasons (i.e. too much compression or stretching). The second limit is the high computational cost of RBF that can be faced using fast solvers which implementation could be delicate and rather complex.

Many interesting researches demonstrating that RBF can be successfully adopted for the deformation of calculation meshes are running. If we look back some years (De Boer *et al.*, 2007; Jakobsson and Amoignon, 2007) we discover very good applications in which the high numerical cost has limited the use of RBF (direct solution grows by N^3 where N is the number of RBF centres). A recent study about mesh morphing using tri-harmonic RBF kernel (Sieger *et al.*, 2014) demonstrates the good potential of the method, but even in this case performances are perceived as a barrier. The first industrial implementation of RBF mesh morphing was introduced in 2009 with the software RBF Morph™ (Biancolini *et al.*, 2009) that comes with a fast RBF solver for the bi-harmonic kernel which performances scales as $N^{1.6}$. A complete description of the tool is given in (Biancolini, 2012).

The RBF mesh morphing technique of the aforementioned software has became the core of the RBF4AERO Project which aims at developing the RBF4AERO Benchmark Technology, an integrated numerical platform and methodology to efficiently face the most demanding challenges of aircrafts design and optimization (RBF4AERO, 2013). This project represents the great occasion to further push and extend the application of mesh morphing in the aviation sector after it received lots of acknowledgments in other industrial field such as automotive (Sovani and Khondge, 2012), motorsport (Caridi and Wade, 2012; Petrone *et al.*, 2014), nautical (Biancolini *et al.*, 2014) and medical (Biancolini *et al.*, 2012). In particular, the intent of RBF4AERO is to cover modern aeronautical design applications such as shape optimization (Biancolini *et al.*, 2013), ice accretion simulation (Biancolini and Groth, 2014), fluid-structure interaction (FSI) (Cella and Biancolini, 2012; Reina *et al.*, 2014), adjoint-morphing coupling and multi-physics optimization analyses through efficient procedures based on RBF mesh morphing such to prevent the typical compromise of standard optimization procedures in terms of speed, accuracy and extent.

Radial Basis Functions

From mathematical point of view, the solution of the RBF problem consists of the calculation of the coefficients of a linear system of order equal to the number source points (De Boer *et al.*, 2007), by means of which the displacement of an arbitrary mesh's node can be expressed, and then imposed, as the summation of the radial contribution of each source node. In such a way, mesh smoothing can be rapidly applied by maintaining mesh topology in terms of total number and type of elements.

In particular, the RBF Morph tool utilises the RBF interpolant **s** composed by a radial function containing the RBF φ and a multivariate polynomial corrector vector **h** of order *m-1*, where *m* is said to be the order of φ, introduced with the aim to assure the compatibility for rigid motions. Specifically, if *N* is the total number of source points, the formulation of the RBF interpolant is

$$\boldsymbol{s}(\boldsymbol{x}) = \sum_{i=1}^{N} \boldsymbol{\gamma}_i \varphi\left(\left\|\boldsymbol{x} - \boldsymbol{x}_{\boldsymbol{k}_i}\right\|\right) + \boldsymbol{h}(\boldsymbol{x}) \qquad (1)$$

where **x** is the vector identifying the position of a generic node belonging to the surface and/or volume mesh, $\boldsymbol{x}_{\boldsymbol{k}_i}$ is the i-th source node position vector and $\|\bullet\|$ is the Euclidean norm.

The RBF fitting solution exists in case the RBF coefficients vector $\boldsymbol{\gamma}_i$ and the weights of the polynomial corrector vector $\boldsymbol{\beta}_i$ can be found such that, at source points, the interpolant function possesses the specified (known) values of displacement $\mathbf{g}_i$, whilst the polynomial terms give a null contribution, namely the following relations are simultaneously verified

$$\boldsymbol{s}\left(\boldsymbol{x}_{\boldsymbol{k}_i}\right) = \boldsymbol{g}_{\boldsymbol{i}} \qquad 1 \le i \le N \qquad (2)$$

$$\sum_{i=1}^{N} \boldsymbol{\gamma}_i q\left(\boldsymbol{x}_{\boldsymbol{k}_i}\right) = 0 \qquad (3)$$

for all polynomials *q* with a degree less than or equal to that of polynomial **h** (Beckert and Wendland, 2001). The minimal degree of polynomial $\boldsymbol{h}$ depends on the choice of the RBF type. It can be demonstrated that a unique RBF interpolant exists if the RBF is conditionally positive definite (Van Zuijlen *et al.*, 2007). In the case that this latter condition is established and if the order is less than or equal to 2 (Jin *et al.*, 2001), a linear polynomial applies

$$\boldsymbol{h}(\boldsymbol{x}) = \boldsymbol{\beta}_{\boldsymbol{1}} + \boldsymbol{\beta}_{\boldsymbol{2}} x + \boldsymbol{\beta}_{\boldsymbol{3}} y + \boldsymbol{\beta}_{\boldsymbol{4}} z \qquad (4)$$

enabling to exactly recover rigid body translations.

In the event such assumptions are verified, the interpolant has the form

$$\boldsymbol{s}(\boldsymbol{x}) = \sum_{i=1}^{N} \boldsymbol{\gamma}_i \varphi\left(\left\|\boldsymbol{x} - \boldsymbol{x}_{\boldsymbol{k}_i}\right\|\right) + \boldsymbol{\beta}_{\boldsymbol{1}} + \boldsymbol{\beta}_{\boldsymbol{2}} x + \boldsymbol{\beta}_{\boldsymbol{3}} y + \boldsymbol{\beta}_{\boldsymbol{4}} z \qquad (5)$$

and $\boldsymbol{\gamma}_i$ and $\boldsymbol{\beta}_i$ values can be obtained by solving the system

$$\begin{pmatrix} \boldsymbol{M} & \boldsymbol{P} \\ \boldsymbol{P}^T & \boldsymbol{0} \end{pmatrix} \begin{pmatrix} \boldsymbol{\gamma} \\ \boldsymbol{\beta} \end{pmatrix} = \begin{pmatrix} \boldsymbol{g} \\ \boldsymbol{0} \end{pmatrix} \tag{6}$$

where **M** is the interpolation matrix having the elements derived by calculating all the radial interactions between source points as follows

$$M_{ij} = \varphi\left(\left\|\boldsymbol{x}_{\boldsymbol{k}_i} - \boldsymbol{x}_{\boldsymbol{k}_j}\right\|\right) \qquad 1 \le i \le N, \qquad 1 \le j \le N, \tag{7}$$

and **P** is a constraint matrix that arises balancing the polynomial contribution containing a column of 1 and the spatial positions of source points in the remaining three columns, that is

$$\boldsymbol{P} = \begin{pmatrix} 1 & x_{k_1} & y_{k_1} & z_{k_1} \\ 1 & x_{k_2} & y_{k_2} & z_{k_2} \\ \vdots & \vdots & \vdots & \vdots \\ 1 & x_{k_N} & y_{k_N} & z_{k_N} \end{pmatrix}, \tag{8}$$

assuming that source points are not contained in the same plane (otherwise the interpolation matrix would be singular).

For what described, by satisfying the displacement field prescribed at source points, RBF Morph operates the smoothing of mesh nodes using the following formulation of the interpolant

$$\begin{cases} s_x(\boldsymbol{x}) = \sum_{i=1}^{N} \gamma_i^x \varphi\left(\left\|\boldsymbol{x} - \boldsymbol{x}_{\boldsymbol{k}_i}\right\|\right) + \beta_1^x + \beta_2^x x + \beta_3^x y + \beta_4^x z \\ s_y(\boldsymbol{x}) = \sum_{i=1}^{N} \gamma_i^y \varphi\left(\left\|\boldsymbol{x} - \boldsymbol{x}_{\boldsymbol{k}_i}\right\|\right) + \beta_1^y + \beta_2^y x + \beta_3^y y + \beta_4^y z \\ s_z(\boldsymbol{x}) = \sum_{i=1}^{N} \gamma_i^z \varphi\left(\left\|\boldsymbol{x} - \boldsymbol{x}_{\boldsymbol{k}_i}\right\|\right) + \beta_1^z + \beta_2^z x + \beta_3^z y + \beta_4^z z\,. \end{cases} \tag{9}$$

A great flexibility using RBF can be achieved acting on the radial functions that can be compactly or globally supported. Common options are summarized in Table 1. RBF Morph allows 4 radial functions. The distance function (global supported and bi-harmonic in 3D) is used by default and performs very well in volume morphing as it allows to get very good quality and it is accelerated so that it can handle RBF problem beyond 1 million of centres (source points). Wendland functions (C0,C2 and C3) are available for surface sculpting as the high level of continuity can be used to control a surface using just a few control points.

RBF can be used in generic n-dimensional spaces as a tool for the generation of the response surface (Bai *et al.*, 2012); according to past experience (Biancolini *et al.*, 2014) the cubic RBF performs very well in this task.

Table 1 Typical Radial Basis Functions.

Radial Basis Functions (RBF) with global support	$\varphi(r)$
Spline type (R_n)	$r^n, n\ odd$
Thin plate spline (TPS_n)	$r^n \log(r), n\ even$

Multiquadric (MQ)	$\sqrt{1+r^2}$
Inverse multiquadric (IMQ)	$\frac{1}{\sqrt{1+r^2}}$
Inverse quadratic (IQ)	$\frac{1}{1+r^2}$
Gaussian (GS)	e^{-r^2}
Radial Basis Functions (RBF) with compact support	$\varphi(r) = f(\xi), \xi \leq 1, \xi = \frac{r}{R_{sup}}$
Wendland C^0 (C0)	$(1-\xi)^2$
Wendland C^2 (C2)	$(1-\xi)^4(4\xi+1)$
Wendland C^4 (C4)	$(1-\xi)^6\left(\frac{35}{3}\xi^2+6\xi+1\right)$

RBF Morph

RBF Morph is a numerical suite for morphing and shape optimization that combines a very accurate control of the geometrical parameters with an extremely fast mesh deformation capability. It is the first commercial mesh morphing software based on Radial Basis Functions. The tool is an add-on of the CFD code ANSYS® Fluent® and is fully integrated in the solving process.

An overview of the industrial workflows faced using RBF Morph and Fluent has been presented in (Biancolini, 2014). The overall HPC performances of past applications are summarized in Table 2**Error! Reference source not found.**. In all applications but one, shape parameterization (design variables represent the number of shapes blended) is used for optimization purposes in which parameters are varied to evaluate variations of the baseline (design evaluations); IR5-Dallara case is a Fluid-Structure Interaction (FSI) example in which the 5 shapes represent structural modes. The HPC result is summarized by the RUN hours (net time in which the preprocessing time to set up RBF shapes is not considered), that is strongly affected by the number of cores adopted. For this reason, it is interesting to report the serial time for a single design point (Serial Time One Design) and also the serial time per million of cells that is representative of the effort required for the completion of a class of runs. Figures of last row are comparable regardless the size of the mesh and number of cores employed and it can be used to have a quick estimation for a preliminary sizing of the HPC facility suitable for a specific application.

Table 2 HPC performances of past applications handled through RBF Morph. Present study is in the last column.

Case	Motorbike windshield	Reference car estate	Sedan	Hull	Volvo XC60	Sails	DLR-F6	IR5	Taurus
Organization	MRA / UTV	MIRA	ANSYS	Leeds	ANSYS	NewCastle / UTV	Morph Lab / UTV	Dallara	Pipistrel
Year	2009	2010	2011	2011	2012	2013	2013	2013	2014
Mesh dimension (mill.)	1.5	5.2	6	0.3	50	1,5	14	80	7
Mesh type	Tets	poly	tets	hexa	tets	hexa	tets	tets	Hexa
Design variables	3	3	2	8	4	4	8	5	2
Design evaluations	45	27	9	45	50	100	81	1	25
Optim. environment	modeFrontier	Mathcad	DX	DX	DX	Mathcad	DX	FSI	DX+Mathcad
CPU	4	2	12	4	240	16	16	256	20
RUN (hr)	48	300	24	45	50	26	102	1	64
Time to set-up one par (hr)	1.5	2.5	2.0	1.0	2.0	2.0	1.0	2.0	0.5
Time to set-up (hr)	4.5	7.5	4.0	8.0	8.0	8.0	8.0	8.0	1.0
Serial time one design (hr)	4.3	22.2	32.0	4.0	240.0	4.2	20.2	256.0	51.2
Serial time one design (hr/Mcells)	2.8	4.3	5.3	13.3	4.8	2.8	1.4	3.2	7.3

The meshless nature of the morphing approach makes it easily configurable for other mesh formats. As such, the software is also available as a standalone library to be coupled with any code. In fact, the morphing field can be applied directly embedding the morphing operation in the targeted solver (OpenFOAM® is an example) or acting on the file that stores nodal position (CFD++®, elsA and Nastran® are other examples of successful coupling). This means that multi-

physics optimisation can be implemented using morphing field to bring all the mesh related to physics simulated onto the same current shape.

Mesh to CAD

Mesh morphing operations usually produce new geometries available just as meshes. This occurs in two scenarios. The most common one, that is the case of the application presented in this paper, is when the parametric geometry is defined directly at mesh level using RBF modelling tools. But there are other situations in which new shapes are sculpted using information known on a point by point basis on the original surface mesh (or eventually on an overlapped not-matching one). Among them we recall the adjoint solver sensitivities, ice/snow accretion profiles and structural deformations coming from Finite Element Model (FEM) analyses. A mechanism to regenerate a Computer-Aided Design (CAD) representation of the new surfaces is then required.

The tool currently implemented in the mesh morphing software RBF Morph has the capability to work with CAD data conforming to the Standard for the Exchange of Product Data (STEP) format protocol and can be controlled by the user directly acting in a dedicated panel available on the software graphical user interface (GUI). It simply applies the morphing field used for the mesh to all the points stored in the step file (CAD morphing).

The method is not exact, that means some discrepancies between the mesh and the generated CAD can be observed at the end of the process. Such errors is in our experience very small and the morphed mesh can be easily updated to exactly conform CAD output if a final check is required. The method is not based on a total CAD regeneration but rather on a synchronization of the CAD surfaces and the mesh. It works very well with morphing operations because topology is preserved in the mesh and it can be preserved, accordingly, on the Boundary Representation (BREP) representation of surfaces. It takes the advantage of the meshless character of the RBF approach and foresees that the control points defining the geometry are moved employing the same morphing solution computed to modify the numerical grid. This means that, similarly to mesh morphing, on the one hand the CAD module needs to be fed with the original baseline geometry and, on the other hand, the RBF solution can be the result of a combination of whatever number of single RBF solutions.

This approach works if the baseline geometry is flexible enough to represent new desired shape. We control this flexibility performing a Non-Uniform Rational Basis Spline (NURBS) transformation of all the surfaces to be updated. The operation can be straightforwardly automated using the CAD modeller and the degree of flexibility is guaranteed with the refinement of NURBS, *i.e.* acting on the number of points uniformly spaced in u and v parametric directions of the original surfaces.

In Figure 2 an example of the described approach is demonstrated on a 90 degree angle bent tube in which an overlay of the mesh and CAD geometries for the original (left) and final (center) configurations is represented. The morphing action

was obtained as a result of an adjoint driven optimization and applied to both the models by using the same calculated solution. To better showcase the quality of the optimized geometry, in Figure 2 (right) are also reported the relative errors introduced by the mesh to CAD process with respect to the original tube diameter, demonstrating a maximum error lower than 5% in correspondence of the red areas.

Figure 2 Mesh to CAD method applied to a 90 degree angle bent tube.

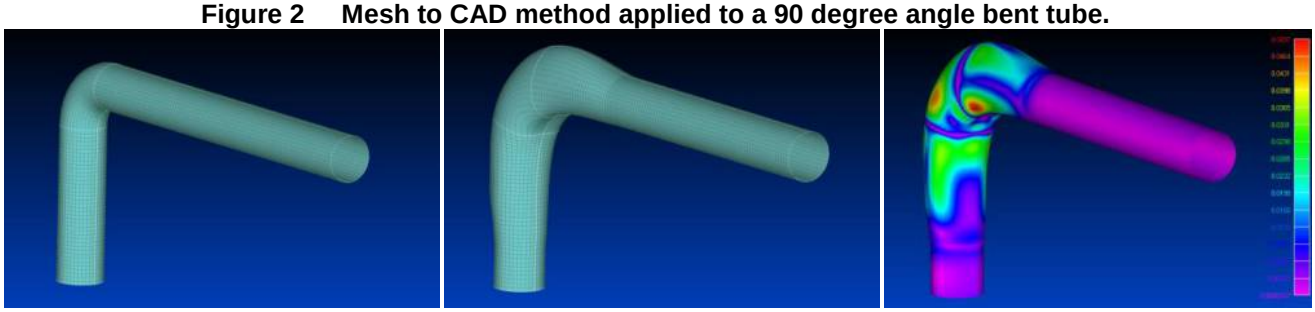

Description of the optimization procedure

The workflow of the optimization procedure proposed in the present work is illustrated in Figure 3 through a block diagram. In the chart, rectangular blocks represent computational data, circular blocks identify specific operations or features, whilst blocks dealing with the use of the same tool are included in a coloured region.

Figure 3 Workflow of the mesh morphing based shape optimization.

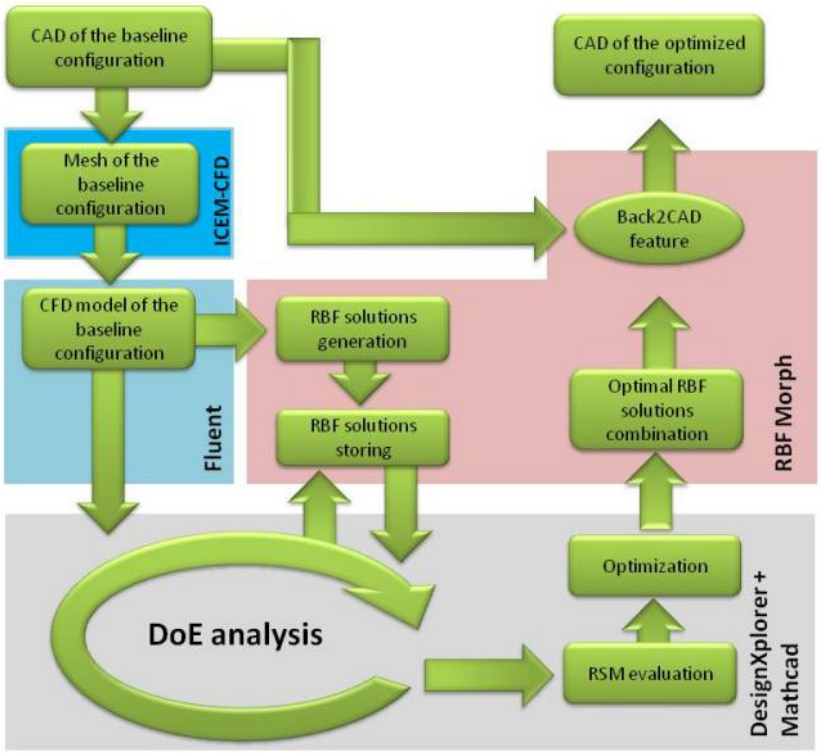

The workflow, in this specific study managed using ANSYS® Workbench™ environment and Mathcad™ software, foresees the availability of the CAD representing the baseline configuration of the model to be studied, and provides, as final output, the CAD model of the optimized shapes. In particular, the operations characterised by the highest level of

automation are those performed by means of ANSYS® DesignXplorer™ (DX) which acts as driver of the entire optimization procedure. DX supports the sequential accomplishment of the main phases of the optimization which begins with the definition of the design of experiment (DoE) table and prosecutes with the design points (DPs) evaluation. The entries of the table are the combinations of RBF solutions (design variables) amplification values and the corresponding objective functions deriving from the design point analysis. As soon as the DoE table is completed, its data can be processed and visualized using a Response Surface Method (RSM). We used cubic RBF implemented in Mathcad for this specific task. The optimization algorithm can then identify the optimal combination of RBF solutions that, applied to the baseline CAD model, generates the mathematics of the optimal design. The latter achievement is obtained by morphing the starting CAD by the back2CAD feature of RBF Morph.

The proposed procedure can be effortlessly implemented using different environments. The automation can be steered using general optimisation tools as modeFrontier® and Dakota or custom optimiser developed using high level tools, such as Mathcad or Microsoft® Excel®, and/or programming/scripting languages such as bash, Python, C or MATLAB®.

Application on an aircraft shape optimization problem

The described optimization procedure was applied on a typical aeronautical design problem, namely the improvement of the aerodynamic performance of a glider in manoeuvring at high altitude.

Problem description

The Taurus glider, designed and manufactured by Pipistrel d.o.o. Ajdovščina Slovenia (Figure 4 and Figure 5), is a side-by-side two-seat self-launching ultra-light glider made out of composite materials. The wing is located in a vertical central position respect to the fuselage, whilst its longitudinal position is aft the maximum section, behind the cockpit, in a positive pressure gradient region.

Figure 4 The Taurus glider.

This configuration implies that, in the wing/fuselage junction, the wing suffers an extra increase of flow velocity close to the leading edge and a significant adverse pressure gradient in the trailing edge region that cause a leading edge

separation at high angles of attach (AoAs). The problem is mainly felt when lowering the Reynolds number (increasing the altitude) effecting a drastic decreasing of the overall aircraft aerodynamic efficiency in manoeuvring.

Figure 5 Taurus three view representation.

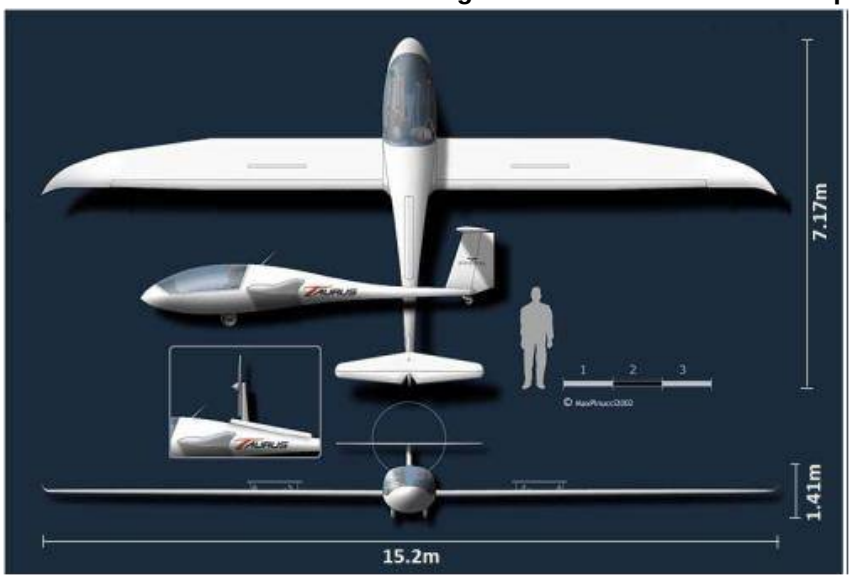

The occurrence of such flow conditions was demonstrated experimentally by performing flight tests (Figure 6). The flow attachment on glider's surface was monitored by means of small rectangular pieces of adhesive tape - tufts. Unordered direction of tufts at the wing/fuselage fairing clearly indicates a detached flow that is propagating according to a delta shape in the streamwise direction.

The objective of the work is to apply the shape optimization procedure in order to diminish such a separation and consequently enhance the aerodynamic efficiency of the aircraft.

Figure 6 Snapshot of the flow detachment.

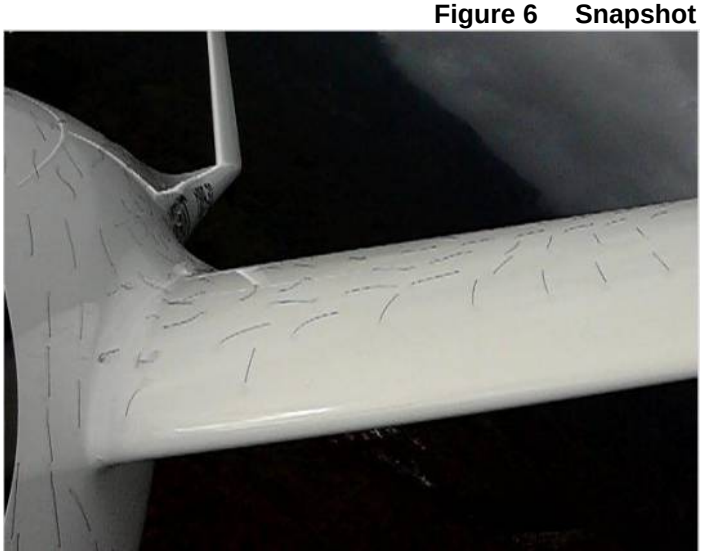

This study is part of a set of explorative analyses that aimed at anticipating the investigation of the proper shape modifications to be applied in view of carrying out the scheduled computational applications of the RBF4AERO Project (RBF4AERO, 2013).

Analysis of the baseline geometry

The CAD model of the glider was provided by Pipistrel. In order to reduce the computational effort it consists of a simplified version of the real aircraft in which only the areas of interest are accurately reproduced (winglets and tail are not modelled).

Assuming the symmetry of the flow field, the mesh models just half domain. The grid is multi-block structured hexahedral and it is extended around 40 wing chords upstream the model, 60 downstream and 50 on the side. The dimensions is 7 million. Figure 7 details the cells distribution on wall surfaces.

The analysis was performed at an AoA of 8 deg. The flow conditions are Mach 0.08 and Reynolds 1.24 million (based on reference chord of length 0.8 m) that correspond to the flying condition at 2000 metres of altitude.

An incompressible steady Reynolds-averaged Navier-Stokes equations (RANS) computation was performed using the two equations k-ω Shear Stress Transport (SST) turbulence model (Menter, 1994).

Figure 7 Details of the surface mesh.

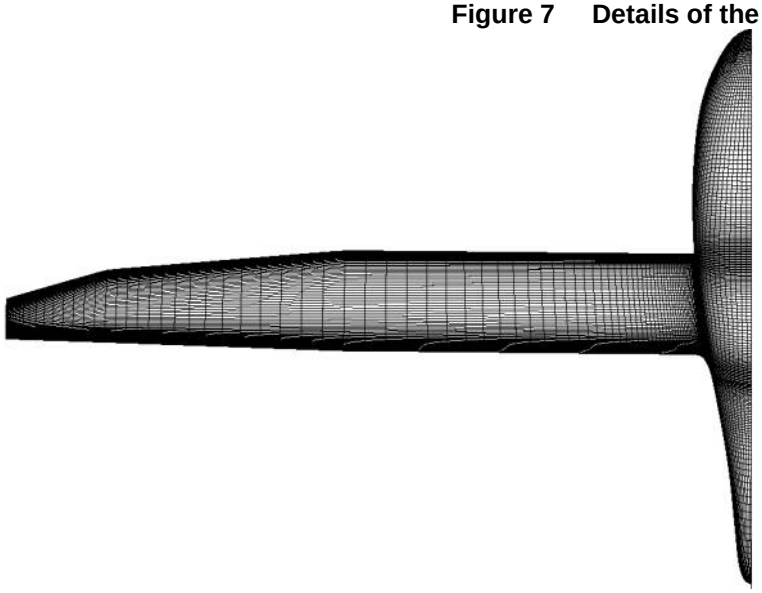

A steady pressure based solver, with SIMPLE scheme for pressure-velocity coupling and Second Order Upwind scheme for spatial discretization, was employed. The coefficients convergence was reached after 5000 (

Figure 8).

Figure 8 Aerodynamic coefficients convergence histories (C_L and C_D).

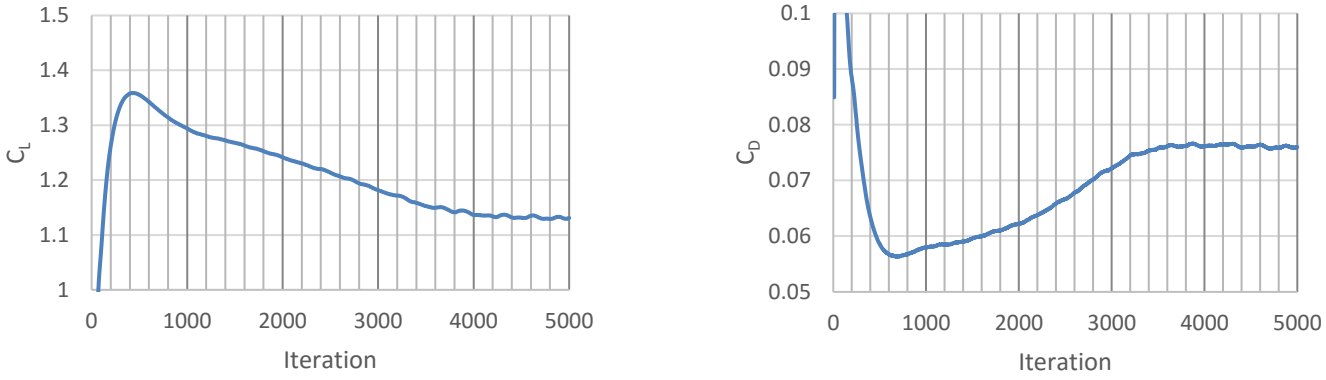

The cells are clustered on the wall surfaces in order to solve the boundary layer up to the wall with the dimension growth rate in the order of 1.2. The Figure 9 reports a contour plot of the Y+ distribution on the glider model.

Figure 9 Wall Y+ distribution.

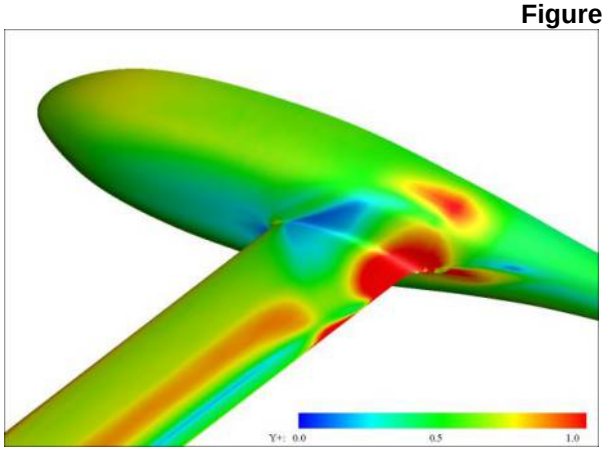

The regions of the model experiencing flow detachment is shown in Figure 10 by the visualization of the shear stress streamlines superposed on skin friction coefficient distribution. As visible, the physical phenomenon registered during the experimental flight is numerically reproduced and confirmed.

Figure 10 Streamlines superposed on skin friction coefficient distribution for baseline configuration.

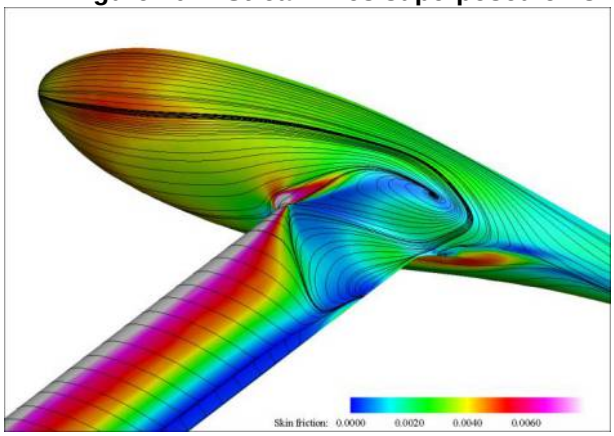

RBF setup

Two shape modifications acting on the wing/fuselage junction, respectively nearby the leading edge and trailing edge, were set up. The shape modifiers, that are the mathematical framework enabling the RBF solutions computing, for both modifications were generated using the Surfs and Encaps features of RBF Morph (RBF Morph, 2014). In particular, one Surf set was used to fix the nodes that are required not to change their position, two cylinder-shaped Moving Encaps to deform the glider's surfaces and one box-shaped Domain Encap to delimit the extension of the morphing action. The location of the source nodes generated by the described set-up is shown in Figure 11, whilst the effect produced on the geometry by the application of the generated solutions is shown in Figure 12.

Figure 11 Source nodes position of the RBF morphing problem.

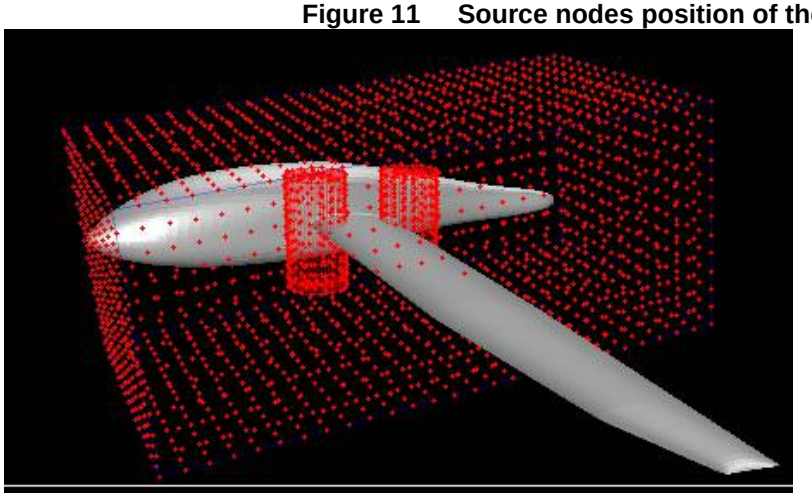

It is interesting to notice that, thanks to the meshless nature of the RBF morphing action, any sculpting strategy can be implemented. In this specific example we have decided to use one of the approaches recommended in the modelling best practices of RBF Morph (RBF Morph, 2014) in which two cylindrical bodies located at a proper distance from the surface act as sculpting tool imposing a space warping that allows to remodel the junction.

Figure 12 Shape deformation induced by shape modifiers.

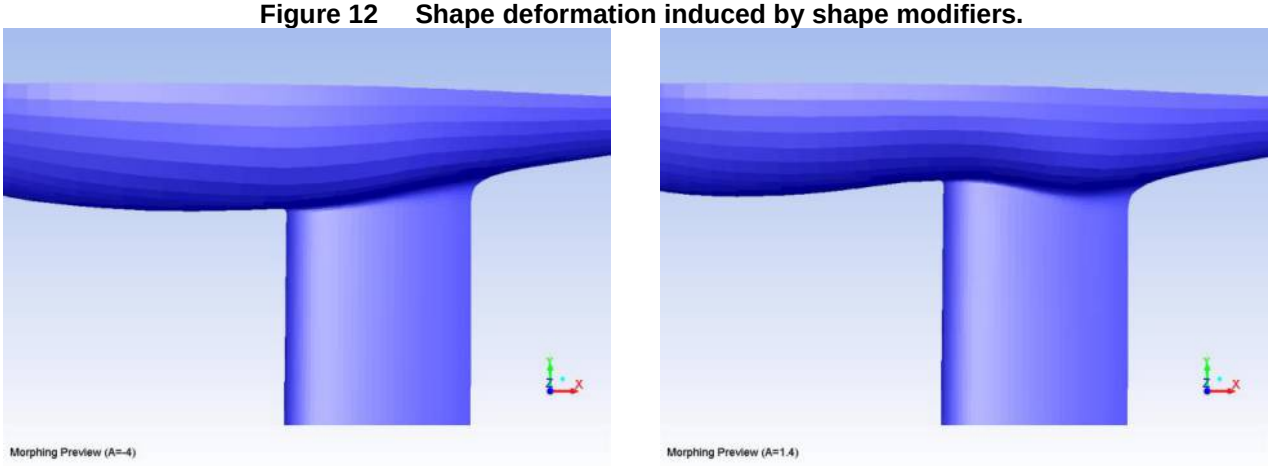

The same RBF morphing action will be applied, at the end of the optimization process, to the baseline CAD model in order to generate the mathematics of the selected optimal candidate.

Optimization solutions

After the RBF configuration setup, the computation of the morphing solutions and their storage are envisaged to be carried out. A parametric grid, whose shape modifications can be amplified according to the optimization parameters, is now ready and available to the CFD code. The analysis block is suitable to be integrated in the optimization loop. As already introduced, the optimization strategy applied in this work consisted of the definition of a DoE table, its completion with the design points objective functions evaluation and the subsequent generation of a RS (Response Surface) on which to applying the optimization criterion. The table was populated with 25 design points: the first 20 points were defined using a Latin hypercube sampling design method and successively other 5 extra points were added to enrich the design space in the most interesting area. The aerodynamic efficiency ($E=C_L/C_D$) is the objective function of the optimization.

The amplification of the RBF solution acting near the leading edge is linked to the input named P1 with an allowable range [-0.4;1.4]. The amplification for the trailing edge is linked to the input parameter P2 with a range [-4;5]. The limits of both modifiers should be defined according to the best practice taking into account for detrimental effects on mesh quality. The quality of morphed meshes has been investigated before the calculation. For this specific case we have noticed that the quality peak (minimum registered orthogonal quality is 6.92332e-03) does not change after morphing for any combination of the shape parameters. This means that the critical area, concerning mesh quality, is not interested by the morphing action, and it is preserved even after mesh deformation.

In order to speed up the DoE table completion, all DPs analyses were ran restarting the computation from the already achieved baseline solution and then morphed according to the imposed input parameters.

It is worth to comment how the RS method can be used to continuously improve the knowledge about a specific system. In the present study we are evaluating each DP using high fidelity runs. Sampling strategy was previously tuned and refined using a coarser mesh for the evaluation of each design point (Costa *et al.*, 2014) . Despite the quantitative differences observed when the same point is evaluated using the finer and the coarser meshes, the relevant design area stays more or less the same; in Figure 13 and Figure 14 RS post processing coming from the dataset obtained using the coarser mesh are provided to be easily compared. It is worth to notice that the trend registered in the efficiency is similar but the coarser model foresees a lower value. The difference between the high fidelity model and the coarse one is in the range [12%;18%] in all the design space with an average value of 15% and a scatter with respect to average value in the range [-3%;+3%].

For the DoE table post processing we have developed in house a code based on RBF method. The obtained RS dealing with the aerodynamic efficiency is depicted in Figure 13. The squared points on the surface are the solutions of the DoE table. A screening approach on the RBF metamodel has been adopted to generate a finely spaced cloud of design points (3600 individuals) according to a full-factorial approach. Notice that the negligible cost of RS evaluation makes affordable this granular screening of the RS even using millions of DPs.

Figure 13 Response Surface represented as a scatter plot. The plot on the left is the one obtained using the high fidelity model. The plot on the right is obtained using a coarse mesh (Costa *et al.*, 2014).

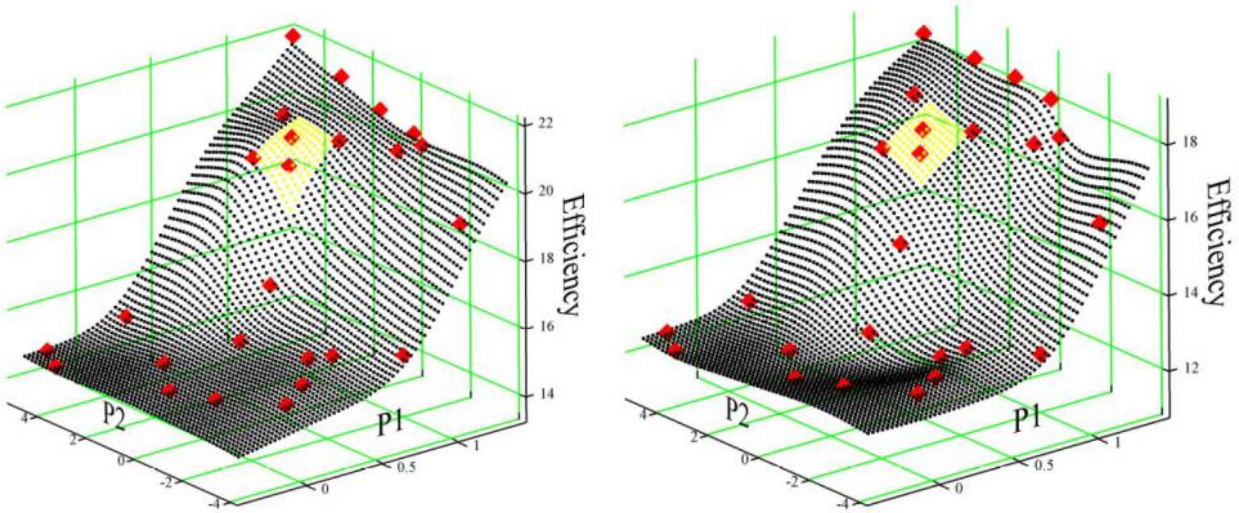

The upper design space border exhibits the highest efficiency portion of the RS highlighting a higher sensitivity of the objective function from the leading edge modifier (P1) with respect to the trailing edge one (P2). No global maximum was reached inside the domain. This behaviour is aerodynamically justified considering that the trailing edge shape modifier has no effects if leading separation occurs. When the leading edge parameters acts on the fuselage, preventing the leading edge stall, the trailing edge parameters begins to be effective reducing the adverse pressure gradient (and the trailing edge separation).

Optimal candidate selection and CAD geometry generation

Two design variables were adopted in this work. The RSM solution is then a three dimensional surface. Furthermore, a very regular and monotonic RS was obtained. The optimization problem is then quite simple for any algorithm and the definition of the best candidate is quite straightforward. The selection of the optimum was then additionally subjected to practical manufacturing evaluations. According to the RS obtained and to the impact that the shape modifiers have on the geometry, it was considered a reasonable compromise to limit the parameters amplification in order to squeeze the fuselage of an amount not larger than about 10 centimetres from the baseline geometry. The consequence of such a constraint is to focus the research of the optimum in the light area of the RS reported in Figure 13. A high accuracy of the RS is expected in this subset where five computed design points should ensure a good agreement between the metamodel and the objective function. We can also notice that in the area in which the first parameter is upper bounded,

the second parameter exhibits a quite flat behaviour. A better insight can be gained cutting the RS at aforementioned bound, as shown in Figure 14. From this section we can notice that an area in which the efficiency exhibits a higher rise begins at P2 = 1.5 and reaches the highest efficiency at P2 = 3, after that an almost flat behaviour is observed. For this reason we have selected P2 = 2.5 as optimal candidate (dotted line in Figure 14).

Figure 14 Section of Response Surface at P1=1. The "fine" curve is the one obtained using the high fidelity model. The "coarse" one is obtained using a coarse mesh (Costa *et al.*, 2014).

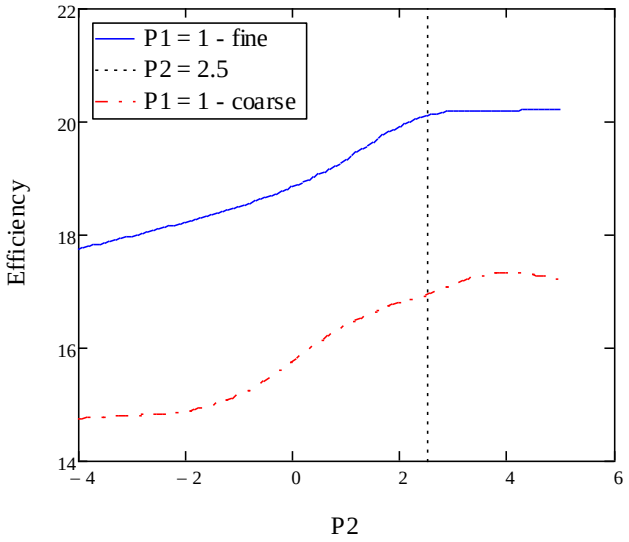

It is worth to notice that the selected optimum (P1 = 1; P2 = 2.5) is very close to a computed design point. Its performance could then be trusted even without repeating the CFD computation. Nevertheless, for completeness, we have validated it with a new analysis of the geometry generated applying the combination for the amplification values defined as optimal design. The solution of the analysis is reported in Figure 15. The significant reduction of separation obtained respect to the baseline geometry (Figure 10) is evident.

Figure 15 Streamlines superposed on skin friction coefficient distribution for the optimized configuration.

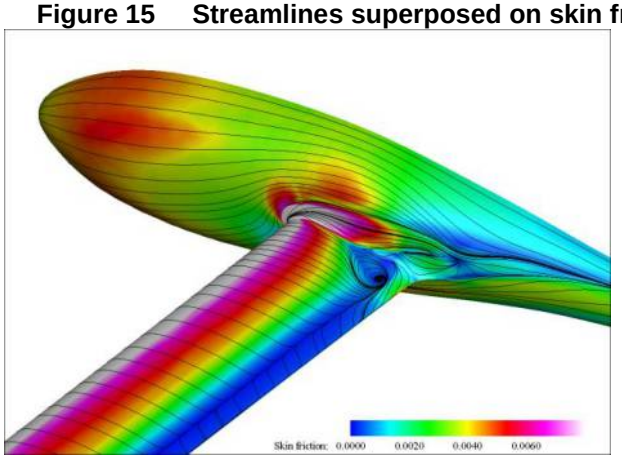

The improvement obtained can be also appreciated comparing the pressure distribution on the baseline and on the optimized geometry. In Figure 16 the pressure coefficient profiles at different sections of the wing for both geometries are plotted. In particular, the sections of interest are those on the first 10% of the span. The separated region and its spanwise extent is clearly evidenced by the pressure plateau evolution.

Figure 16 Pressure coefficient profiles along wing sections for baseline and optimised configurations.

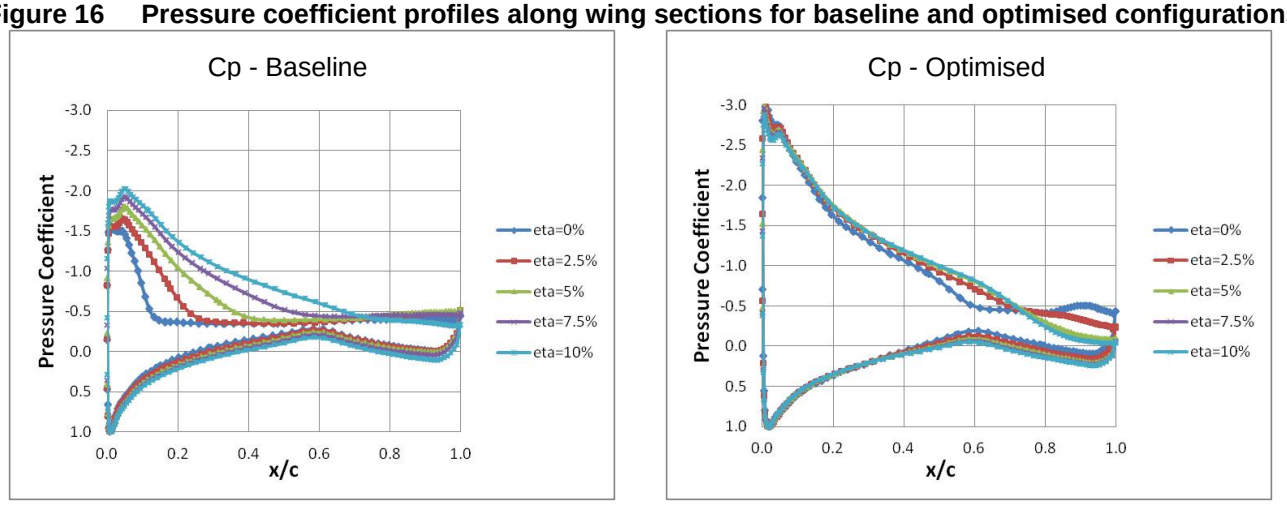

In Table 3 the aerodynamic coefficients of the baseline and the obtained optimal solutions are summarized. The aerodynamic efficiency of the optimized configuration is relevantly improved (35%).

Table 3 Main results related to aerodynamic coefficients.

Parameter	Baseline	Optimised	Variation
C_D	0.076	0.0605	-20.4%
C_L	1.131	1.216	+7.5%
E	14.88	20.1	+35.0%

As a completion of the design process, the back2CAD feature of the RBF Morph was used to apply the morphing action, amplified in accordance to the parameters of the optimized solution, to the baseline CAD model (in STEP format) in order to generate the geometric mathematics of the new solution. Figure 17 shows the resulting CAD model.

Figure 17 CAD model of the optimized configuration.

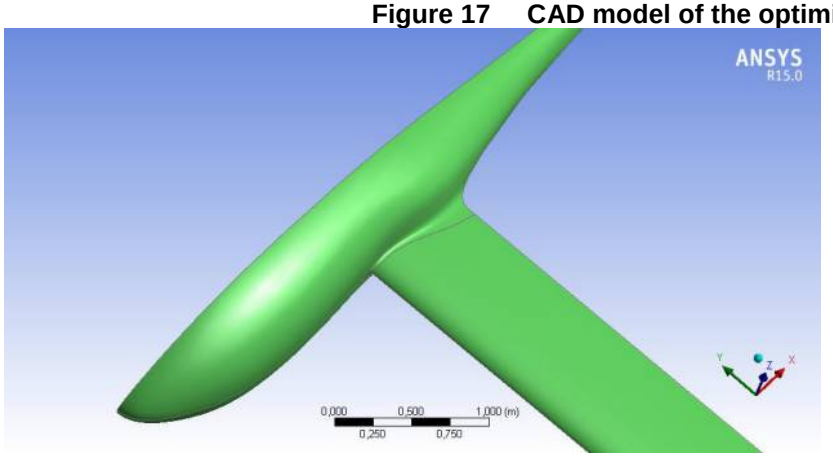

Performances of the proposed workflow

The numerical workflow was executed using a small server (dual processor Xeon E5-2680 2.8 GHz, 20 cores, 128 Gb RAM). Achieved performances are summarized in the last column of Table 2. The total time required for the complete workflow was 64 hours, we can notice that the Serial time for one design normalized for one million of cells is 7.31. Moreover, we can predict that the overall time needed to compute the complete DoE table, composed by 25 DPs, can be reduced at a target of 5 hours using 240 cpu. In this scenario the time spent updating the mesh according to the prescribed shape modifications was calculated to be 19 seconds and thus it can be neglected.

Using the same facility, the past workflow based on the coarse mesh required 13 hours for the evaluation of the DOE and 5 extra hours for the high fidelity computation at baseline point and optimal point. The overall CPU demand was 18 hours against the 64 hours required for the full high fidelity analysis.

The performance gain using this approach becomes substantially higher if the workflow is compared with a standard one in which the parametric mesh is not available and so a new mesh needs to be generated for each design point. Using morphing the mesh is generated once; the updating cost is very small and can be neglected. The time for the set-up of shape parameters time is in any case required (for RBF or using a CAD software). So the gain is given by the meshing time required for each new mesh (including manual stage if any). In the hypothesis of a mesh generation time equal to 4 hours the standard workflow becomes 160 hours (4*24 hours of meshing added) against 70 (4 hours of meshing added).

Conclusions

A numerical optimization procedure based on mesh morphing techniques was developed and applied to a typical aeronautical design problem. The method consists of the parameterization of the computational domain using RBF Morph, a morphing software based on Radial Basis Functions fully integrated within the CFD computational environment. The selection of the optimum was performed on a RS generated by a cubic RBF interpolation of the design points of a predefined DoE table.

The procedure was applied for the improvement of the efficiency of a glider which suffers of a wing leading edge flow separation close to the fuselage when manoeuvring at high altitude. The optimization problem was setup defining two design variables that act as shape modifiers in the wing root leading edge and trailing edge regions. The obtained RS allowed, according to reasonable manufacturing constraints, to select a candidate that showed to significantly improve the performance of the aircraft, in the test conditions, without modifying the wing geometry but only affecting the fuselage shape. The new geometry evidenced only a small trailing edge separation with a 35% of aerodynamic efficiency improvement respect to the baseline configuration of the vehicle. The process was completed generating the CAD model

of the optimized solution applying the RBF morphing action to the baseline CAD mathematics according to the set-up and the amplification factors resulting from the optimization.

The CFD numerical configuration was set up following best practice rules in facing such kind of analysis. The boundary layer was solved up to the wall and a fine domain composed of 7 million of cells was used. Even if we were solving large separated flow regions, the procedure showed to be very robust and efficient. We could adopt such an accurate CFD model because our problem was not very demanding from the optimization point of view. In our case only 25 design points were sufficient to model the objective function. However, such kind of procedures can become very demanding if a large number of design variables are adopted. In such cases, the computational costs can be rather expensive also within large HPC environment and particular care has to addressed in selecting the opportune accuracy/costs compromise if dealing with realistic engineering problems. A previous work published by the authors on this test case evidenced the possibility to obtain similar results with a much cheaper computational resource requirements (Costa, et al., 2014). RS data of the past study are provided demonstrating that the optimal design area can be properly identified; nevertheless, as the difference in the trend shows a scatter in the range [-3%;+3%], the location of the optimal point requires in any case an exploration of such design area using the high fidelity model and so a mixed approach that switches to the high fidelity model in the final stage could be the best compromise between accuracy and performances.

Acknowledgments

This work was financially supported by the RBF4AERO Project, funded in part by the European Union 7th Framework Programme (FP7-AAT, 2007 - 2013) under Grant Agreement no. 605396. To get further information, please visit the RBF4AERO's website at www.rbf4aero.eu.

References

Bai, Y. C., Han, X., Jiang, C. and Liu, J. (2012), "Comparative study of metamodeling techniques for reliability analysis using evidence theory", *Advances in Engineering Software*, November 2012, Volume 53, pp. 61–71.

Beckert, A. and Wendland, H. (2001), "Multivariate interpolation for fluid-structure-interaction problems using radial basis functions", *Aerospace Science and Technology*, 5(2), pp. 125-134.

Biancolini , M.E. (2012), "Mesh Morphing and Smoothing by Means of Radial Basis Functions (RBF): A Practical Example using Fluent and RBF Morph", in *Handbook of research on computational science and engineering: theory and practice*, IGI Global.

Biancolini , M.E., Biancolini, C., Costa, E., Gattamelata, D. and Valentini, P.P. (2009), "Industrial application of the meshless morpher RBF morph to a motorbike windshield optimisation", in EASC 2009 Proceesings of the 4th European Automotive Simulation Conference, Germany, 6-7 July 2009, Munich, Germany.

Biancolini , M.E., Cella, U., Travostino, G. and Mancini, M. (2013), "Shaping up – Mesh morphing reduces the time required to optimize an aircraft wing", *ANSYS Advantage Magazine*, VII, Issue 1, pp 32-34.

Biancolini , M. E. and Groth, C. (2014), "An Efficient Approach to Simulating Ice Accretion on 2D and 3D Airfoils", *Advanced Aero Concepts, Design and Operations Applied Aerodynamics Conference 2014*, 22-24 July, Bristol, UK.

Biancolini , M. E., Ponzini, R., Antiga, L. and Morbiducci, U. (2012), "A new workflow for patient specific image-based hemodynamics: parametric study of the carotid bifurcation", *Conference CompImage 2012*, 5 September 2012, Rome, Italy.

Biancolini , M. E., Viola, I. M. and Ramirez, S. (2014), "Alla ricerca delle regolazioni ottimali di una barca a vela mediante il mesh morphing", *Analisi & Calcolo*, May/June, Issue 63, pp. 12-18.

Biancolini , M. E., Viola, I. M. and Riotte, M. (2014), "Sails trim optimisation using CFD and RBF mesh morphing", *Computers and Fluids*, 10 April, pp. 46–60.

Biancolini, M. E. (2014), Automotive Simulation World Congress 2014. Tokyo, Japan.

Buhmann, M. D. (2003), *Radial Basis Functions*, New York, Cambridge University Press.

Caridi, D. and Wade, A. (2012), "Higher-Speed CFD", *Professional Motorsport World Magazine*, April-June 2012, p.56.

Cella, U. and Biancolini, M.E. (2012), "Aeroelastic Analysis of Aircraft Wind-Tunnel Model Coupling Structural and Fluid Dynamic Codes", *AIAA Journal of Aircraft*, March–April, Vol. 49, No. 2 (2012), pp. 407-414.

Costa, E., Biancolini M.E., Groth, C., Cella, U., Veble G and Andrejasic M. (2014), "Ottimizzazione aerodinamica di un aliante industriale mediante l'utilizzo di RBF", *Analisi & Calcolo*, September/October 2014, Issue 64, pp. 36-46.

Costa, E., Biancolini M.E., Groth, C., Cella, U., Veble, G. and Andrejasic, M. (2014), "RBF-based aerodynamic optimization of an industrial glider", in *30th International CAE Conference*, Pacengo del Garda, Italy.

De Boer, A., van der Schoot, M. S. and Bijl, H. (2007), “Mesh deformation based on radial basis function interpolation”, *Computers & Structures*, 85(11–14), pp. 784–795.

Jakobsson, S. and Amoignon, O. (2007), “Mesh deformation using radial basis functions for gradient based aerodynamic shape optimization”, *Computers & Fluids*, 36(6), pp. 1119–1136.

Jin, R., Chen, W. and Simpson, T. W. (2001), “Comparative Studies of Metamodelling Techniques under multiple Modelling Criteria”, *Structural and Multidisciplinary Optimization*, Volume 23, pp. 1–13.

Menter, F.R. (1994), “Two-Equation Eddy-Viscosity Turbulence Models for Engineering Applications”, *AIAA Journal*, August, 32(8), pp. 1598-1605.

Petrone, G., Hill, C. and Biancolini, M.E. (2014), “Track by Track Robust Optimization of a F1 Front Wing using Adjoint Solutions and Radial Basis Functions”, *32nd AIAA Applied Aerodynamics Conference*, June 2014, Atlanta, Georgia, USA.

RBF4AERO, 2013, “Innovative benchmark technology for aircraft engineering design and efficient design phase optimisation, available at: http://www.rbf4aero.eu/ (accessed 10 December 2014).

RBF-Morph (2014), “RBF Morph - Users Guide”.

Reina, G.P, Della Sala, A., Biancolini, M.E., Groth, C., Caridi, D. (2014), ”Store Separation: Theoretical Investigation of Wing Aeroelastic Response”, *4th Aircraft Structural Design Conference*, 7-9 October 2014, Belfast, Northern Ireland.

Sieger, D., Menzel, S. and Botsch, M. (2014), “RBF morphing techniques for simulation-based design optimization”, *Engineering with Computers*, April, 30(2), pp. 161-174.

Sovani, S. and Khondge, A. (2012”, “Scaling New Heights in Aerodynamics Optimization: The 50:50:50 Method”, available at: http://www.ansys.com (accessed 10 December 2014).

Van Zuijlen, A. H., De Boer, A. and Bijl, H. (2007), “Higher-order time integration through smooth mesh deformation for 3D fluid–structure interaction simulations”, *Journal of Computational Physics*, 224(1), pp. 414–430.

Nomenclature

Symbols

Name	Description	Units
C_p	Pressure coefficient	-
C_D	Drag coefficient	-
C_L	Lift coefficient	-
h	Generic polynomial	Units of $\boldsymbol{g}$
n	Dimensions of the design space	-
N	Number of RBF centres	-
q	Generic polynomial	Units of $\boldsymbol{g}$
r	Distance between two points	Units of $\boldsymbol{x}$
Re	Reynolds number	-
s	Interpolation function composed of an RBF and a polynomial	Units of $\boldsymbol{g}$
s_x, s_y, s_z	Components of the morphing field	m, m, m
$\boldsymbol{g}$	Vector of the scalar function to be interpolated, evaluated at RBF centres	Units of parametric space (m for morphing)
$\boldsymbol{x}$	Position vector in the Cartesian reference system *O(x,y,z)*	Units of parametric space (m for morphing)
$\boldsymbol{x_k}$	Vector of RBF centres	Units of $\boldsymbol{x}$
$\boldsymbol{M}$	Interpolation matrix used for RBF fit	-
$\boldsymbol{P}$	Constraint matrix used for RBF fit	-
φ	Radial Basis Function	-
$\boldsymbol{\beta}$	Vector of coefficients of the fitted polynomial	-
$\boldsymbol{\gamma}$	Vector of coefficients of the fitted RBF	-

Definitions, Acronyms and Abbreviations

AoAs	angle(s) of attach
BREP	Boundary Representation
CAE	Computer-Aided Engineering
CAD	Computer-Aided Design
CFD	Computational Fluid Dynamics
CPU	Central Processing Unit
DoE	Design of Experiments
DPs	design point(s)
FSI	Fluid-Structure Interaction
FEM	Finite Element Model
HPC	High Performance Computing
NURBS	Non-Uniform Rational Basis Spline
RAM	Random-access memory
RANS	Reynolds-averaged Navier-Stokes
RBF	Radial Basis Functions
RS(M)	Response Surface (Method)
SST	Shear Stress Transport
DX	ANSYS® DesignXplorer™
Mathcad	Mathcad™
Fluent	ANSYS® Fluent®